Novel Chiroptical Spectroscopy Technique

Jorge Olmos-Trigo,[1,*] Cristina Sanz-Fernández,[2] and Ivan Fernandez-Corbaton[3]
[1]Departamento de Física de Materiales, Universidad Autónoma de Madrid, 28049 Madrid, Spain
[2]Centro de Física de Materiales (CFM-MPC), Centro Mixto CSIC-UPV/EHU, Manuel de Lardizabal 4, 20018 San Sebastián, Spain
[3]Institute of Nanotechnology, Karlsruhe Institute of Technology, 76021 Karlsruhe, Germany

(Received 25 June 2025; revised 9 February 2026; accepted 2 March 2026; published 24 June 2026)

Chiral objects typically exhibit a different extinction for the two circular polarizations of light. Researchers often detect the chirality of objects by measuring this extinction difference employing circular dichroism spectroscopy. In this Letter, we present a new spectroscopy technique for detecting the chirality of dipolar objects based on measuring the Stokes parameters at any nonforward angle. The chirality measure we introduce effectively eliminates achiral background noise and is independent of both the object's concentration and the optical path length. Notably, when a solution contains both enantiomers of a chiral object, our method can discern which enantiomer predominates. Furthermore, we demonstrate that the technique is robust and verifiable *in situ* by measuring the Stokes vector at two different nonforward angles of choice.

DOI: 10.1103/crdw-pxcs

Introduction—Chirality refers to the geometric property of objects that cannot be superimposed onto their mirror images. In nature, chirality is ubiquitous; numerous organic molecules, such as glucose, and most biological amino acids are chiral. In the pharmaceutical industry, chiral specificity is crucial as opposite enantiomers, mirror pairs of chiral molecules, can have vastly different effects on biological systems depending on their handedness [1]. Enantiomer pairs share the same atomic composition and are indistinguishable when measuring their scalar molecular properties. It is through interactions with other chiral entities that their chirality can be revealed.

In nanophotonics, the electromagnetic helicity is the most commonly used chiral entity to unveil the chirality of objects [2]. Circular dichroism (CD) spectroscopy stands as the most utilized technique to unveil molecular chirality using helicity [3,4]. In a conventional CD setup, the molecular solution is sequentially illuminated with fields of opposite helicities, and the total transmitted power is recorded for each case. The CD signal is then computed by taking the difference between these two power measurements in transmission, the forward direction of the light-scattering system.

Despite its widespread commercial use, CD exhibits drawbacks. For instance, if CD $= 0$ for a given frequency of the incident electromagnetic field, it is indeterminate whether the molecular solution is chiral or not. This ambiguity arises because CD provides only partial information about the chirality of the molecule [3]. To overcome this limitation and gain more insights into the chiral nature of the molecular solution, researchers typically measure optical rotation (OR), which quantifies the change of the polarization direction when linearly polarized light propagates through a chiral medium [3]. However, both CD and OR are measured in the forward direction, which presents a challenge: the presence of a large achiral background signal that hinders the accuracy and reliability of measurements. Moreover, CD and OR depend on molecular concentration and optical path length, which makes their signature for a given chiral object nonuniversal.

In this Letter, we introduce a novel spectroscopy technique for detecting the chirality of dipolar objects, modeled as spherical nanoparticles and nanohelices, based on measuring the Stokes parameters at nonforward angles.

The chirality measure that we introduce is universal, and in particular, avoids the achiral background and is independent of the object's concentration and the optical path length. Additionally, when the solution presents both enantiomers of a chiral object, our polarimetry-based method can discern which enantiomer predominates in the solution.

Importantly, we demonstrate that our technique is robust, and its accuracy can be experimentally verified *in situ* by measuring the Stokes parameters at two different nonforward angles of choice.

Our findings pave the way to characterize the chirality of objects beyond CD and OR, the current state-of-the-art chiroptical spectroscopy techniques.

The setting—The interaction between the electromagnetic field and a small object, such as most chiral

*Contact author: jolmostrigo@gmail.com

molecules, can be treated in the linear dipolar approximation. This relates a 6×6 polarizability tensor with the incident electric and magnetic fields $\{\mathbf{E}_{\mathrm{inc}}(\mathbf{r}), Z\mathbf{H}_{\mathrm{inc}}(\mathbf{r})\} \in \mathbb{C}^3$ at the position of the object, $\mathbf{r} = \mathbf{r}_0$, with the induced electric and magnetic dipolar moments, denoted as $\mathbf{p}(\mathbf{r}_0)$ and $\mathbf{m}(\mathbf{r}_0)$, respectively,

$$\begin{pmatrix} \mathbf{p}(\mathbf{r}_0)/\epsilon \\ Z\mathbf{m}(\mathbf{r}_0) \end{pmatrix} = \begin{pmatrix} \bar{\alpha}_{\mathrm{ee}} & \bar{\alpha}_{\mathrm{em}} \\ \bar{\alpha}_{\mathrm{me}} & \bar{\alpha}_{\mathrm{mm}} \end{pmatrix} \begin{pmatrix} \mathbf{E}_{\mathrm{inc}}(\mathbf{r}_0) \\ Z\mathbf{H}_{\mathrm{inc}}(\mathbf{r}_0) \end{pmatrix}. \quad (1)$$

Here, all $\bar{\alpha}_{\mathrm{ij}}$ are 3×3 complex-valued tensors, and ϵ and $Z = \sqrt{\mu/\epsilon}$ denote the electric permittivity and impedance of the surrounding medium, respectively. Note that the electric $\bar{\alpha}_{\mathrm{ee}}$, magnetic $\bar{\alpha}_{\mathrm{mm}}$, and chiral $\bar{\alpha}_{\mathrm{em,me}}$ polarizabilities have dimensions of volume in our formulation. A harmonic time dependence $\exp(-\mathrm{i}\omega t)$ is assumed and suppressed from the notation. The $\bar{\alpha}_{\mathrm{ab}}$ tensors are frequency dependent, as are some other quantities, but we only write such dependence later.

At this point, it is very often assumed that the rotationally averaged response of a dipolar object can be approximated by the response of an isotropic dipolar object [5–7]. It is important to realize that such an approximation is typically good if and only if such a response is evaluated in the forward direction. At nonforward angles, this approximation generally does not hold. An exception to this rule is a spherical nanoparticle, which is the system we next consider. We should also mention that the spherical chiral model, derived by Bohren in 1974 [8], is one of the most used frameworks for studying chiral light-matter interactions [9–24]. Given all these considerations, we express Eq. (1) as

$$\begin{pmatrix} \mathbf{p}(\mathbf{r}_0)/\epsilon \\ Z\mathbf{m}(\mathbf{r}_0) \end{pmatrix} = \begin{pmatrix} \alpha_{\mathrm{ee}}\bar{I} & \alpha_{\mathrm{em}}\bar{I} \\ -\alpha_{\mathrm{em}}\bar{I} & \alpha_{\mathrm{mm}}\bar{I} \end{pmatrix} \begin{pmatrix} \mathbf{E}_{\mathrm{inc}}(\mathbf{r}_0) \\ Z\mathbf{H}_{\mathrm{inc}}(\mathbf{r}_0) \end{pmatrix}, \quad (2)$$

where $\bar{I}$ is the 3×3 identity matrix. For scalars, as is the case, we have used that $\alpha_{\mathrm{em}} = -\alpha_{\mathrm{me}}$ because of reciprocity [25]. Upon interaction with the incident field, dipoles typically reradiate. The field scattered by an electric and magnetic dipole can be written in the radiation (far-field) zone as [26]

$$\mathbf{E}_{\mathrm{sca}}(\mathbf{r}) = k^2 \frac{e^{ikr}}{4\pi r} \left[\left(\hat{\mathbf{e}}_{\mathrm{r}} \times \frac{\mathbf{p}(\mathbf{r}_0)}{\epsilon} \right) \times \hat{\mathbf{e}}_{\mathrm{r}} - (\hat{\mathbf{e}}_{\mathrm{r}} \times Z\mathbf{m}(\mathbf{r}_0)) \right]. \quad (3)$$

Here, $\hat{\mathbf{e}}_{\mathrm{r}}$ is the radial unit vector, k is the radiation wave number, and $r = |\mathbf{r} - \mathbf{r}_0|$ denotes the observation distance to the center of the dipolar object.

Next, we introduce the Stokes vector and assume $\mathbf{r}_0 = 0$ in the induced dipoles and in the incident field.

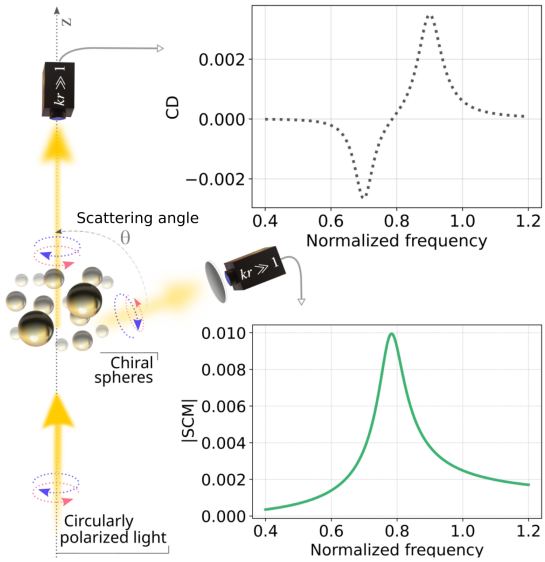

FIG. 1. Chiral sphere sequentially illuminated by electromagnetic fields of opposite helicities. Two chiral observables are recorded: circular dichroism (CD) and Stokes chirality measure (SCM) using a Stokes vector measurement at any nonforward scattering angle, denoted in the figure by θ.

The Stokes vector measurement—The Stokes vector $\mathbf{S} = [s_0, s_1, s_2, s_3]$ describes the polarization state in the far field [27]. The components of the Stokes vector, often referred to as the Stokes parameters [28,29], can be measured using conventional optical components such as a photodetector and wave plates [30]. Following Crichton and Marston's notation [see Eqs. (9a-d) of Ref. [28]], the Stokes parameters read as

$$s_0 = |E_\theta|^2 + |E_\varphi|^2, \qquad s_1 = |E_\theta|^2 - |E_\varphi|^2, \quad (4)$$

$$s_2 = -2\Re\{E_\theta E_\varphi^*\}, \qquad s_3 = 2\Im\{E_\theta E_\varphi^*\}. \quad (5)$$

Here, s_0 is the total scattered intensity, s_1 is the degree of linear polarization, s_2 is the degree of linear polarization at 45°, and s_3 denotes the degree of circular polarization. Note that θ and φ denote the scattering and azimuth angles in spherical coordinates, respectively. A sketch of the light-scattering system is depicted in Fig. 1. In this regard, we use the same angle conventions as in Ref. [28].

At this point, we have all the ingredients to calculate the polarizabilities as a function of the Stokes parameters given in Eqs. (4) and (5). We will assume that the solution is subsequently illuminated by two incident plane waves that differ only by their helicity. That is, by their circular polarization handedness $\sigma = \pm 1 : Z\mathbf{H}_{\mathrm{inc}}(\mathbf{r}) = -\mathrm{i}\sigma\mathbf{E}_{\mathrm{inc}}(\mathbf{r})$ [2]. Expanding Eqs. (4) and (5) using Eqs. (2) and (3) we can get an equation (see Supplemental Material Sec. S1 [31]) of the form $\mathbf{J}^{\sigma}_{\mathrm{sph}} = \bar{U}^{\sigma}_{\mathrm{sph}}(kr, \theta)\mathbf{S}^{\sigma}(kr, \theta)$, where

$$N\begin{pmatrix}|\gamma^\sigma|^2\\ |\beta^\sigma|^2\\ \Re\{\gamma^\sigma(\beta^\sigma)^*\}\\ \Im\{\gamma^\sigma(\beta^\sigma)^*\}\end{pmatrix}=\bar{U}^\sigma_{\rm sph}(kr,\theta)\begin{pmatrix}s^\sigma_0(kr,\theta)\\ s^\sigma_1(kr,\theta)\\ s^\sigma_2(kr,\theta)\\ s^\sigma_3(kr,\theta)\end{pmatrix}. \quad (6)$$

Here, we have defined

$$\gamma^\sigma=\alpha_{\rm ee}-{\rm i}\sigma\alpha_{\rm em},\qquad \beta^\sigma=\alpha_{\rm mm}-{\rm i}\sigma\alpha_{\rm em}, \quad (7)$$

and N is the number of illuminated objects. We anticipate that knowing N is not needed as it will cancel out in the definition of our novel chirality measure. Equation (6) is the first important results of this Letter. The quadrivector $\mathbf{J}^\sigma_{\rm sph}$, accounting for all quadratic combinations of the helicity-dependent polarizabilities $\{\gamma^\sigma,\beta^\sigma\}$, can be captured from a measurement of the Stokes vector $\mathbf{S}^\sigma(kr,\theta)$ evaluated at a single scattering angle θ in the far field. As Eq. (6) shows, one only needs to apply a simple 4×4 matrix $\bar{U}^\sigma_{\rm sph}(kr,\theta)$ to the measurement of $\mathbf{S}^\sigma(kr,\theta)$ to obtain $\mathbf{J}^\sigma_{\rm sph}$. It is important to note that $\mathbf{J}^\sigma_{\rm sph}$ does not depend on the amplitude of the incident field E_0, which cancels out. In addition, the optical distance from the center of the sample to the observational point, denoted by kr, does not modify $\mathbf{J}^\sigma_{\rm sph}$ as long as $\mathbf{S}^\sigma(kr,\theta)$ is measured in the far field. This is because $\mathbf{S}^\sigma(kr,\theta)\propto(kr)^{-2}$, canceling the $(kr)^2$ dependence in Eq. (6).

We now discuss how to use Eq. (6) in the optical laboratory.

By inspecting Eq. (S14) of Supplemental Material Sec. S1 [31], we note that the θ can be freely chosen in the interval $0<\theta<\pi$, where $\csc^4\theta\neq0$. This holds since $\mathbf{J}^\sigma_{\rm sph}$ does not depend on the choice of θ. Nevertheless, one must avoid any propagation direction where the incident field has a component. Otherwise, the total field measured in the optical laboratory will be the sum of the scattered and incident fields, thus invalidating Eq. (6). Moreover, it is important to note that the angle φ does not play any role in Eq. (6) since the system is symmetrical in azimuth. Thus, φ can be chosen freely in the optical laboratory.

Additionally and regarding the fidelity of our method, we highlight that it is robust upon two measurements of the Stokes vector at distinct observational points. That is, if we apply Eq. (6) for two different angles θ_1 and θ_2 and obtain the same $\mathbf{J}^\sigma_{\rm sph}$, then our method is reliable. Otherwise, it indicates that the setting we assumed is not valid. Such a practical consistency check is valuable in the optical laboratory.

A novel chiroptical spectroscopy technique—We start this section by considering the difference, $\mathbf{D}=\mathbf{J}^+_{\rm sph}-\mathbf{J}^-_{\rm sph}$, and the sum, $\mathbf{S}=(\mathbf{J}^+_{\rm sph}+\mathbf{J}^-_{\rm sph})/2$, quadrivectors,

$$\mathbf{D}=\mathbf{J}^+_{\rm sph}-\mathbf{J}^-_{\rm sph}=N\begin{pmatrix}4\Im\{\alpha^*_{\rm ee}\alpha_{\rm em}\}\\ 4\Im\{\alpha^*_{\rm mm}\alpha_{\rm em}\}\\ 2\Im\{(\alpha_{\rm ee}+\alpha_{\rm mm})^*\alpha_{\rm em}\}\\ 2\Re\{(\alpha_{\rm ee}-\alpha_{\rm mm})^*\alpha_{\rm em}\}\end{pmatrix}, \quad (8)$$

$$\mathbf{S}=\frac{\mathbf{J}^+_{\rm sph}+\mathbf{J}^-_{\rm sph}}{2}=N\begin{pmatrix}|\alpha_{\rm ee}|^2+|\alpha_{\rm em}|^2\\ |\alpha_{\rm mm}|^2+|\alpha_{\rm em}|^2\\ \Re\{\alpha_{\rm ee}\alpha^*_{\rm mm}\}+|\alpha_{\rm em}|^2\\ \Im\{\alpha_{\rm ee}\alpha^*_{\rm mm}\}\end{pmatrix}. \quad (9)$$

We note that if any of the four components of $\mathbf{D}$ is different from zero, the object is chiral, namely, $|\alpha_{\rm em}|\neq0$. There is, however, one exception to this rule: the first Kerker condition $\alpha_K=\alpha_{\rm ee}=\alpha_{\rm mm}$ [32–34] combined with the phase constrain $\Im\{\alpha_K\alpha^*_{\rm em}\}=0$. In this unconventional case, additional observables may be required to determine the presence of chirality at a fixed frequency ω of the incident field. Moreover, if $\alpha_{\rm em}=0$, then we recover the Stokes vector method for achiral objects [35,36].

Importantly, this exceptional condition is not specific to dipolar spherical objects but rather reflects a general feature of scattering by chiral spherical objects, independent of their optical size. If the object is dual-symmetric [2] and satisfies the phase constraint, the scattering cross section becomes independent of the helicity of the incident field. Consequently, despite being chiral, the object responds identically to left- and right-handed incident helicities at nonforward angles and effectively behaves as an achiral scatterer. A detailed discussion can be found in Supplemental Material Sec. S2 [31]. We highlight that this exceptional condition is not met by chiral molecules because their magnetic polarizabilities are many orders of magnitude below their electric polarizabilities.

Having noted these points, we now discuss the underlying physics for $\mathbf{D}\neq0$. If we know that the sample is a solution containing the two versions of a given chiral object, we can further detect which enantiomer is more abundant in the solution. This is evidenced by the change in sign of $\mathbf{D}$ depending on the specific enantiomer. Note that for two enantiomers i and j of the same chiral object, we have $\alpha^i_{\rm em}=-\alpha^j_{\rm em}$.

Many different chirality measures can be derived from $\mathbf{D}$. We now present one of the most interesting ones. We call our quantity the Stokes chirality measure (SCM), defined as

$$\mathrm{SCM}=2\left[\frac{\mathbf{D}(4)-{\rm i}\mathbf{D}(1)/2}{\mathbf{S}(1)+\mathbf{S}(2)}\right]. \quad (10)$$

Expanding Eq. (10) using Eqs. (7)–(9), we get

$$\mathrm{SCM}=4\left[\frac{\Re\{(\alpha_{\rm ee}-\alpha_{\rm mm})^*\alpha_{\rm em}\}-{\rm i}\Im\{\alpha^*_{\rm ee}\alpha_{\rm em}\}}{|\alpha_{\rm ee}|^2+2|\alpha_{\rm em}|^2+|\alpha_{\rm mm}|^2}\right]. \quad (11)$$

The SCM is unitless due to the division by $\mathbf{S}(1)+\mathbf{S}(2)$, which can be seen as the total "size squared" of the polarizability tensor. To be more explicit, if $\mathbf{S}(1)+\mathbf{S}(2)=0$, then the object is transparent to any incident field [29]. In this vein, we note that the imaginary part of the SCM can also be obtained as $2(\mathbf{D}(3)-\mathbf{D}(2)/2)/(\mathbf{S}(1)+\mathbf{S}(2))$. An average of the two expressions should reduce the noise when the SCM is obtained from laboratory measurements.

At this stage, we place our novel findings in the context of current technologies. In particular, the SCM given in Eq. (11) can be determined from the hierarchical self-assembly of chiral molecules on the surfaces of metal [37–42] and dielectric achiral spherical nanoparticles [21,43,44]. This is because the chiral molecules can impart their optical activity to the achiral spherical nanoparticles, and this chirality transfer is fully encoded in α_{ee}, α_{em}, α_{mm} of the hybrid nanostructure. Such a chirality transfer technique is increasingly employed, as the CD and OR are significantly enhanced compared with those observed in the absence of the achiral nanoparticles.

However, Eq. (6) may not be accurate in the case of bare chiral molecules in solution, especially when these are highly anisotropic. To address this limitation, we now derive the Stokes vector method for chiral molecules using one of the most employed frameworks for them: the chiral helix model introduced by Jaggard [45]. To achieve this goal, we take the rotationally averaged Stokes vector $\langle S\rangle$ produced by N helices described by the polarizability tensor given in [45][see Eqs. (3) and (4)]. After some algebra (see Supplemental Material Sec. S3 [31]), we arrive at $\mathbf{J}^{\sigma}_{\mathrm{helix}}=\bar{U}^{\sigma}_{\mathrm{helix}}(kr,\theta)\mathbf{S}^{\sigma}(kr,\theta)$, namely,

$$\begin{pmatrix} |\zeta_\sigma|^2 \\ |\eta_\sigma|^2 \\ \Re\{\zeta_\sigma\eta_\sigma^*\} \\ \Im\{\zeta_\sigma\eta_\sigma^*\} \end{pmatrix} = \bar{U}^{\sigma}_{\mathrm{helix}}(kr,\theta)\begin{pmatrix} s_0^{\sigma}(kr,\theta) \\ s_1^{\sigma}(kr,\theta) \\ s_2^{\sigma}(kr,\theta) \\ s_3^{\sigma}(kr,\theta) \end{pmatrix}. \quad (12)$$

Here. we have defined

$$\zeta^{\sigma}=\chi_{ee}-\mathrm{i}\sigma\chi_{em}, \qquad \eta^{\sigma}=\chi_{mm}-\mathrm{i}\sigma\chi_{em},$$

where χ_{ee}, $-\chi_{mm}$, and $\chi_c=-\mathrm{i}\lambda\chi_{em}$ are the polarizabilities given in Ref. [45]. Here, λ corresponds to the right-handed (left-handed) helix; that is, λ specifies the enantiomeric form of the chiral molecule. Equation (12) is a key result of this Letter. The quadrivector $\mathbf{J}^{\sigma}_{\mathrm{helix}}$ can be obtained by applying the matrix $\bar{U}^{\sigma}_{\mathrm{helix}}(kr,\theta)$ [see Eq. (S40)] to the measured $\mathbf{S}^{\sigma}(kr,\theta)$. Equations (6) and (12) are closely analogous; they differ only in the connecting matrix, which reflects the specific geometry of the chiral scatterer (chiral sphere or helical molecule). Importantly, the mathematical form of $\mathbf{J}^{\sigma}_{\mathrm{helix}}$ and $\mathbf{J}^{\sigma}_{\mathrm{sph}}$ is identical. This means that all chirality measures defined for chiral spherical nanoparticles [for instance, Eqs. (8)–(11)] can be directly obtained for chiral helices by substituting $\alpha_{ee}\to\chi_{ee}$, $\alpha_{em}\to\chi_{em}$, and $\alpha_{mm}\to\chi_{mm}$. This fact implies that the SCM remains a well-defined chiral measure for chiral molecules modeled as chiral helices.

We now compare the SCM given in Eq. (11) with standard OR and CD spectroscopy measurements.

Results—A model of the dipolar chiro-optical response is needed for computing examples of the chirality measures. We will use the quasistatic model for the dipolar resonance of a chiral object from [[6], Eq. (20)], which assumes that the electric and magnetic dipolar moments originate from the same current distribution. Under such assumptions, the frequency-dependent polarizability of each resonance can be written as

$$\begin{pmatrix} \alpha_{ee}(\omega) & \alpha_{em}(\omega) \\ -\alpha_{em}(\omega) & \alpha_{mm}(\omega) \end{pmatrix} = A(\omega)\begin{pmatrix} 1 & \mathrm{i}s_{\mathrm{res}}\sqrt{\tau_{\mathrm{res}}} \\ -\mathrm{i}s_{\mathrm{res}}\sqrt{\tau_{\mathrm{res}}} & \tau_{\mathrm{res}} \end{pmatrix}, \quad (13)$$

where

$$A(\omega)=\frac{A_{\mathrm{res}}}{1-\left(\frac{\omega}{\omega_{\mathrm{res}}}\right)^2-\mathrm{i}\frac{\gamma_{\mathrm{res}}\omega}{\omega_{\mathrm{res}}^2}}.$$

Here, ω_{res} is the resonance frequency, γ_{res} determines the linewidth, $\tau_{\mathrm{res}}\geq 0$, and $s_{\mathrm{res}}=\{-1,+1\}$ determines the handedness of the resonance. Opposite enantiomers will feature opposite signs of s_{res}. When $\tau_{\mathrm{res}}=0$, the resonance is purely electric and there is no chiral response. Now, the CD of an isolated resonance at $\omega=\omega_{\mathrm{res}}$ is [7] [Eq. (12)]

$$\mathrm{CD}(\omega_{\mathrm{res}})=-s_{\mathrm{res}}\frac{4\sqrt{\tau_{\mathrm{res}}}}{1+\tau_{\mathrm{res}}}, \quad (14)$$

where the sign has been flipped for a more convenient comparison with the typical expression of CD in a transmission measurement. Equation (14) helps in selecting relevant values of τ_{res}. For example, for chiral molecules the largest values of CD in electronic, vibrational, and rotational CD spectroscopy are of the order 10^{-1}, 10^{-3}, and 10^{-5}, respectively, and the typical values are at least an order of magnitude lower in each case [46–48]. We will consider systems with multiple resonances, and add the polarizabilities of each resonance to obtain the total polarizability tensor of the object.

The following expressions are often used for the CD and OR in the forward direction {see, e.g., [[49], Eqs. (1.2.5), (1.2.8)]},

$$\mathrm{CD}(\omega)=-2\frac{e^{-k(\omega)L\Im\{n_+(\omega)\}}-e^{-k(\omega)L\Im\{n_-(\omega)\}}}{e^{-k(\omega)L\Im\{n_+(\omega)\}}+e^{-k(\omega)L\Im\{n_-(\omega)\}}}, \quad (15)$$

$$\mathrm{OR}(\omega)=k(\omega)L\Re\{n_+(\omega)-n_-(\omega)\}, \quad (16)$$

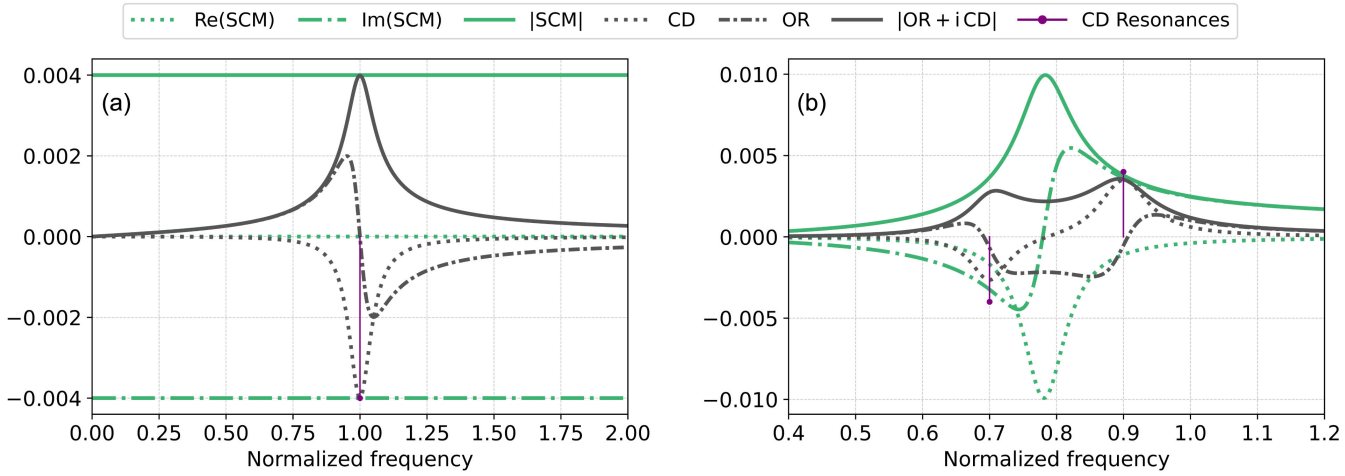

FIG. 2. Stokes chirality measure (SCM), circular dichroism (CD), and optical rotation (OR), calculated with Eqs. (11), (15), and (16), respectively. The CD of each isolated resonance computed with Eq. (14) is shown as purple stem bars. The frequency axis is normalized to 500 THz. All the quantities are dimensionless. (a) Single CD resonance at $\omega/\omega_{\mathrm{res}} = 1$ with $s_{\mathrm{res}} = 1$. (b) Two CD resonances at $\omega/\omega_{\mathrm{res}} = 0.7$ with $s_{\mathrm{res}} = 1$ and $\omega/\omega_{\mathrm{res}} = 0.9$ with $s_{\mathrm{res}} = -1$. In all cases, we consider $\tau_{\mathrm{res}} = 1\mathrm{e}\text{-}6$, $A_{\mathrm{res}} = 2.2727\mathrm{e}\text{-}34$, and $\gamma_{\mathrm{res}}/w_{\mathrm{res}} = 0.1$.

where L is the optical path of the illuminating beam inside the sample, $k(\omega) = \omega/c$, and $n_{\pm}(\omega)$ are the effective refractive indexes for the two helicities of the incident field. Such refractive indexes can be computed using homogenization techniques as {see e.g. [[50], Eq. (6.127)]}

$$
\begin{aligned}
n_{\pm}(\omega) &= \sqrt{\epsilon_r(\omega)\mu_r(\omega)} \pm \kappa(\omega), \\
\epsilon_r(\omega) &= 1 + \frac{4\pi}{3}\frac{N}{V_{\mathrm{int}}}\alpha_{\mathrm{ee}}(\omega), \\
\mu_r(\omega) &= 1 + \frac{4\pi}{3}\frac{N}{V_{\mathrm{int}}}\alpha_{\mathrm{mm}}(\omega), \\
\kappa(\omega) &= \frac{-\mathrm{i}4\pi}{3}\frac{N}{V_{\mathrm{int}}}\alpha_{\mathrm{em}}(\omega),
\end{aligned}
$$

where V_{int} is the volume that they occupy. We have assumed for simplicity, but without loss of generality, that the objects are in vacuum. We also assume $L = 0.01$ m, a beam spot size of area 1 mm^2, with which $V_{\mathrm{int}} = 10^{-8}$ m^3, and a concentration of objects of 1 mg/ml. The value of N depends then on the molecular mass, and we use $N = 2 \times 10^{19}$.

The A_{res} in Eq. (13) remain to be fixed. For a system with a single resonance, A_{res} does not affect the SCM because it cancels out. Its value is, however, needed for computing CD and OR. We have chosen $A_{\mathrm{res}} = 2.2727 \times 10^{-34}$ with the following reasoning. For a system with a single resonance, such value makes the result of Eq. (14) equal to the result of Eq. (15) at $\omega_{\mathrm{res}} = (2\pi)500 \times 10^{12}$, for the relevant values of τ_{res}. Incidentally, the imaginary part of SCM(ω_{res}) coincides as well, as can be seen in Fig. 2(a). We then keep $A_{\mathrm{res}} = 2.2727 \times 10^{-34}$ for all the resonances in the calculations presented in Fig. 2 [51].

Figure 2 shows that the SCM provides a signature of chirality that is different from the typical CD and OR signatures. The case of a single resonance in Fig. 2(a) is the extreme illustration of this point. The frequency-independent behavior of the SCM is, however, a consequence of the model that we use for the polarizability of a chiral resonance, and we do not expect this to be a general property for the SCM of isolated resonances. Figure 2(b) shows the results for the case of two resonances. In this case, while still different, the real and imaginary parts of the SCM are closer to the OR and the CD, respectively. Unsigned measures of chirality, obtained as the absolute values of SCM, and OR + iCD, respectively, are shown in Fig. 2 as well. The unsigned measures enable the detection of chirality. We see from the definitions of their real and imaginary parts, in Eqs. (11), (15), and (16), that their sign flips with the sign of $\alpha_{\mathrm{em}}(\omega)$. Therefore, such real and imaginary parts are suitable for identifying enantiomers.

As we previously anticipated, there is an important difference between SCM, and CD and OR: the value of SCM is independent of the number of excited objects; it only depends on the polarizabilities [Eq. (11)]. This is an advantage over the CD and OR, which depend on the concentration of the species in the solution and the path length [Eqs. (15) and (16)].

In a nutshell, the SCM provides a universal signature of intrinsic chirality for a given chiral object. As such, the SCM captures chiral efficiency rather than pinpointing the spectral location of chiral resonance peaks. This important distinction is shown in Fig. 2(b), where the SCM peak does not coincide with either the CD or OR resonances, as could be expected by comparing Eq. (11) with Eqs. (15) and (16).

An important question arises regarding the actual measurement of SCM, or more generally, the actual

measurement of $\mathbf{J}^{\sigma}$. The question is whether the amount of photons that are scattered in nonforward directions is sufficient for obtaining a signal. Recent experimental work [51] provides us with a reference in this respect. Figure 4 in [51] shows intensity measurements at a scattering angle of 90°. The small error bars indicate that the measurements were reliable. Each point in such measurements was obtained by averaging 10 images taken with an electron multiplying CCD camera, and the concentration of sucrose was 7.3 mol/L. The equivalent continuous wave power of the illumination was on the order of 1 W. Let us assume that the concentration of sucrose would be the one in human blood, which is about 2000 times lower than in the experiment. Assuming a 1 W continuous wave source, we surmise that one would roughly need to average 20 000 pictures to achieve the same measurement reliability. With electron multiplying CCD speeds of many hundreds of pictures per second, such measurement would take on the order of 1 min. Additionally, while a single scattering angle was measured in [51], Eq. (6) would allow one to increase the signal-to-noise ratio and/or reduce the measurement time by combining simultaneous measurements at different scattering angles of collection.

Conclusion—We introduce a spectroscopic technique for detecting the presence and sign of the chirality of dipolar objects, modeled as spherical nanoparticles and nanohelices, based on measuring the Stokes parameters at nonforward directions. Crucially, such measurements are experimentally feasible for chiral molecules [51] and achiral objects [52,53]. Our approach opens a new route to probe chirality beyond the constraints of conventional techniques such as CD and OR, potentially redefining the spectroscopic toolbox for chiral light-matter interactions at the nanoscale.

Acknowledgments—J. O-T. acknowledges financial support from the Spanish Ministry of Science and Innovation (MCIN) and AEI through Project No. PID2022-137569NB-C43. J. O-T. also acknowledges MICINN for the Ramon y Cajal Fellowship (RYC2024-050342-I) and the Junior Leader Fellowship with grant number (LCF/BQ/PR25/12110015) from "La Caixa" Foundation. I. F.-C. acknowledges support by the Helmholtz Association via the Helmholtz program "Materials Systems Engineering" (MSE).

Data availability—The data that support the findings of this study are available from the corresponding author upon reasonable request.

[1] W. Lenz and K. Knapp, Arch. Environ. Health: Int. J. **5**, 14 (1962).
[2] I. Fernandez-Corbaton, X. Zambrana-Puyalto, N. Tischler, X. Vidal, M. L. Juan, and G. Molina-Terriza, Phys. Rev. Lett. **111**, 060401 (2013).
[3] L. D. Barron, *Molecular Light Scattering and Optical Activity* (Cambridge University Press, Cambridge, England, 2009).
[4] S. Adhikari and M. Orrit, ACS Photonics **9**, 3486 (2022).
[5] Y. Tang and A. E. Cohen, Phys. Rev. Lett. **104**, 163901 (2010).
[6] I. Sersic, C. Tuambilangana, T. Kampfrath, and A. F. Koenderink, Phys. Rev. B **83**, 245102 (2011).
[7] P. Scott, X. Garcia-Santiago, D. Beutel, C. Rockstuhl, M. Wegener, and I. Fernandez-Corbaton, Appl. Phys. Rev. **7**, 041413 (2020).
[8] C. F. Bohren, Chem. Phys. Lett. **29**, 458 (1974).
[9] M. Yokota, S. He, and T. Takenaka, J. Opt. Soc. Am. A **18**, 1681 (2001).
[10] A. Canaguier-Durand, J. A. Hutchison, C. Genet, and T. W. Ebbesen, New J. Phys. **15**, 123037 (2013).
[11] A. Hayat, J. B. Mueller, and F. Capasso, Proc. Natl. Acad. Sci. U.S.A. **112**, 13190 (2015).
[12] M. Li, S. Yan, Y. Zhang, Y. Liang, P. Zhang, and B. Yao, Phys. Rev. A **99**, 033825 (2019).
[13] V. Klimov, I. Zabkov, A. Pavlov, and D. Guzatov, Opt. Express **22**, 18564 (2014).
[14] S. Wang and C. T. Chan, Nat. Commun. **5**, 3307 (2014).
[15] M. Kamandi, M. Albooyeh, C. Guclu, M. Veysi, J. Zeng, K. Wickramasinghe, and F. Capolino, Phys. Rev. Appl. **8**, 064010 (2017).
[16] A. A. Sifat, F. Capolino, and E. O. Potma, ACS Photonics **9**, 2660 (2022).
[17] R. Ali, F. A. Pinheiro, R. S. Dutra, T. P. Mayer Alegre, and G. S. Wiederhecker, Phys. Rev. A **108**, 043704 (2023).
[18] T. Kim and Q.-H. Park, Nanophotonics **11**, 1897 (2022).
[19] M. Sadrara and M. Miri, J. Phys. Chem. C **128**, 218 (2023).
[20] Y. Shi, T. Zhu, T. Zhang, A. Mazzulla, D. P. Tsai, W. Ding, A. Q. Liu, G. Cipparrone, J. J. Sáenz, and C.-W. Qiu, Light Sci. Appl. **9**, 1 (2020).
[21] E. Mohammadi, T. Raziman, and A. G. Curto, Nano Lett. **23**, 3978 (2023).
[22] J. Martínez-Romeu, I. Diez, S. Golat, F. J. Rodríguez-Fortuño, and A. Martínez, Nanophotonics **13**, 4275 (2024).
[23] S. Golat, J. J. Kingsley-Smith, I. Diez, J. Martinez-Romeu, A. Martínez, and F. J. Rodríguez-Fortuño, Phys. Rev. Res. **6**, 023079 (2024).
[24] D. Tetour, M. Novotná, J. Tatýrek, V. Máková, M. Stuchlík, C. Hobbs, M. Rezanka, M. Müllerová, V. Setni vcka, K. Dob vsíková *et al.*, Nanoscale **16**, 6696 (2024).
[25] L. Onsager, J. Am. Chem. Soc. **58**, 1486 (1936).
[26] J. D. Jackson, *Classical Electrodynamics* (John Wiley & Sons, New York, 1999).
[27] G. G. Stokes, Trans. Cambridge Philos. Soc. **9**, 399 (1851).
[28] J. H. Crichton and P. L. Marston, Electron. J. Differ. Eqs. **4**, 37 (2000).
[29] J. Olmos-Trigo, M. Nieto-Vesperinas, and G. Molina-Terriza, Phys. Rev. Res. **6**, 043192 (2024).
[30] T. Hinamoto, S. Hotta, H. Sugimoto, and M. Fujii, Nano Lett. **20**, 7737 (2020).
[31] See Supplemental Material at http://link.aps.org/supplemental/10.1103/crdw-pxcs for (S1) derivation of the expression for the Stokes vector for spherical chiral nanoparticles, (S2) discussion of why chiral spherical objects can behave

achirally, and (S3) the Stokes vector for chiral molecules modeled as nanohelices.
[32] M. Kerker, D.-S. Wang, and C. Giles, J. Opt. Soc. Am. A **73**, 765 (1983).
[33] J. Olmos-Trigo, D. R. Abujetas, C. Sanz-Fernández, X. Zambrana-Puyalto, N. de Sousa, J. A. Sánchez-Gil, and J. J. Sáenz, Phys. Rev. Res. **2**, 043021 (2020).
[34] J. Olmos-Trigo and X. Zambrana-Puyalto, Phys. Rev. Appl. **18**, 044007 (2022).
[35] J. Olmos-Trigo, ACS Photonics **11**, 3697 (2024).
[36] J. Olmos-Trigo, Nano Lett. **24**, 8658 (2024).
[37] I. Lieberman, G. Shemer, T. Fried, E. M. Kosower, and G. Markovich, Angew. Chem., Int. Ed. Engl. **47**, 4855 (2008).
[38] J. M. Slocik, A. O. Govorov, and R. R. Naik, Nano Lett. **11**, 701 (2011).
[39] A. O. Govorov and Z. Fan, ChemPhysChem **13**, 2551 (2012).
[40] B. M. Maoz, Y. Chaikin, A. B. Tesler, O. Bar Elli, Z. Fan, A. O. Govorov, and G. Markovich, Nano Lett. **13**, 1203 (2013).
[41] X. Lan, X. Zhou, L. A. McCarthy, A. O. Govorov, Y. Liu, and S. Link, J. Am. Chem. Soc. **141**, 19336 (2019).
[42] A. Paul, M. Venturi, R. Adhikary, G. Salvitti, A. Toma, F. Di Stasio, H. Altug, P. Benassi, D. Tedeschi, C. Ferrante *et al.*, arXiv:2506.15592.
[43] D. Vestler, A. Ben-Moshe, and G. Markovich, J. Phys. Chem. C **123**, 5017 (2019).
[44] N. Siegel, H. Hasebe, G. Chiarelli, D. Garoli, H. Sugimoto, M. Fujii, G. P. Acuna, and K. Kolataj, J. Am. Chem. Soc. **146**, 17250 (2024).
[45] D. Jaggard, A. Mickelson, and C. Papas, Appl. Phys. **18**, 211 (1979).
[46] S. F. Mason, Q. Rev. Chem. Soc. **17**, 20 (1963).
[47] *Measurement of Vibrational Circular Dichroism Spectra Using the FVS-6000* (Jasco International Co., Ltd., 2011).
[48] W. Salzman and P. Polavarapu, Chem. Phys. Lett. **179**, 1 (1991).
[49] L. D. Barron, *Molecular Light Scattering and Optical Activity* (Cambridge University Press, Cambridge, England, 2004), 2nd ed.
[50] A. Sihvola, A. Viitanen, I. Lindell, and S. Tretyakov, *Electromagnetic Waves in Chiral and Bi-Isotropic Media* (Artech House, 1994).
[51] X. Vidal, I. Fernandez-Corbaton, A. F. Barbara, and G. Molina-Terriza, Appl. Phys. Lett. **107**, 211107 (2015).
[52] H. Negoro, H. Sugimoto, and M. Fujii, Nano Lett. **23**, 5101 (2023).
[53] H. Sugimoto, T. Okazaki, and M. Fujii, Adv. Opt. Mater. **8**, 2000033 (2020).